33rd Annual International Conference of the IEEE EMBS
Boston, Massachusetts USA, August 30 - September 3, 2011

The Optimization of an 8-channel Transceive Volume Array for Small Animal MRI at 9.4T

Yu Li[1], Ewald Weber[1], Feng Liu[1], Bing Keong Li[1], and Stuart Crozier[1], *Member, IEEE*

Abstract— **A shielded, non-overlapped 9.4T 8-element transceive volume array was designed and constructed for small animal MRI studies. The coil configuration was optimized to obtain an appropriate trade-off between coil sensitivity, field penetration, and mutual decoupling. The simulated and experimental results presented herein demonstrate that the new volume array is capable of offering higher RF penetration, efficiency and minimum mutual coupling; the proposed technique can also be implemented for a wide range of ultra high-field applications, including dense coil arrays for human studies.**

I. Introduction

Radio frequency (RF) coils play a key role during MRI scanning procedures. In this work, an optimized 8-element transceive volume array is designed and constructed for 9.4T small animal MRI studies.

Ultra-high field small animal MRI systems are widely utilized because they have the advantage of being able to enhance SNR and gain high spectral resolution. Unfortunately, with the move to higher RF-frequencies, the magnetic field within the sample, induced by the RF coil, is highly compromised [1]. Methods such as RF shimming and transmit SENSE have been proposed to circumvent the high-field inhomogeneity problem [2, 3]. To benefit from the advantages of these techniques, dedicated phased array coils with spatially varying transmit-sensitivity of the array elements are essential. However, the beneficial application of these methods is limited by the RF field penetration depth of the individual coil element. This situation becomes even more critical, with the increasing demand for transceive volume arrays to fit the highest feasible number of coil-elements within a given geometry. Any increment of the coil element number will cause the reduction of the aperture size of each coil element; hence the RF penetration depth is sacrificed. Correspondingly, RF signal reception deteriorates within the desired field of view in receive mode.

With an increased number of coil elements, mutual decoupling is harder to control and good channel isolation is difficult to achieve. Several techniques have been introduced to reduce mutual coupling. Overlapping neighbour coils and using low-input impedance preamplifiers [4] can eliminate the extrinsic coupling effectively. Unfortunately, the overlapping sensitivity profile restricts SENSE reconstruction in parallel imaging. Decoupling capacitors or inductors inserted between the nearest neighbour coils can be introduced to minimize the mutual inductance [5, 6]. Although this approach can be extended to a decoupling network to decouple the next nearest neighbour coil [7], these methods are space consuming and too complex to control.

In this paper, an optimized shielded 9.4T 8-element transceive volume array for small animals is proposed to achieve higher RF penetration/efficiency, and minimum mutual coupling. The optimization work is implemented based on the angularly oriented coil blade technique [8] with the consideration of the aforementioned design issues. The optimization strategy mainly includes two aspects: firstly the new design of the coil blade structure; secondly, the refinement of the overall coil configuration. For the coil blade design, a novel 'sandwich' radiating structure is proposed and developed to enhance the coil RF penetration. With the new design, the configurations of the coil structure, including the rotation angle of the coil blade and the aperture size of the coil element, are optimized using a numerical algorithm to minimize the mutual coupling between adjacent coils and further maximise the coil penetration. During the optimization procedure, the sensitivity of the coil in receive mode is considered, in order to improve the performance of the array coil for both transmit and receive situations.

II. Theoretical Analysis of the Optimization Scheme

The available space to place all 8 coil elements of the array is very limited. The entire RF coil and related positioning system need to fit into the standard gradient coil of a Bruker 9.4T Avance III MRI system within a diameter of 116mm. The coil-supporting tube has a length of 90mm in B_0 direction and 75.2mm in diameter. The RF shielding is 200mm long, with an inner diameter of 109mm. The space from the inner tube to the outer shielding former for the RF coil location is only 16.9mm. The Region-of-Interest (ROI) is a cylinder with 43.2mm in diameter and a length of 60mm. With a top view, Fig. 1, 8 loop-elements were circumferentially positioned on the coil former tube [9]. The optimization process includes the designing of the coil blade structure and refining the configuration of the array coil element.

[1]School of Information Technology and Electrical Engineering, University of Queensland, QLD 4072, Australia (e-mail Yu Li: yuli@itee.uq.edu.au).

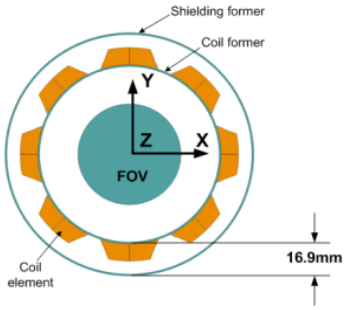

Figure 1 Transverse view of the coil geometry

A. *Optimization of the coil blade design*

The coil element introduced by Weber et al. [8], is assembled with a microstrip-structured blade. This double-surface strip conductor forms a uniformly distributed capacitor along the blade, so that the charge density is distributed on both sides of the conductor surface. Hence, the surface current of the resonant circuit spread on the whole width of the blade. By angularly orienting these wide strip conductors, the effective aperture size of the coil elements become larger and the leakage flux, which cut across neighbour coils, is reduced. Therefore, maximum penetration can be achieved with the minimum mutual coupling. However, in terms of the basic electromagnetic relationship between current source and target magnetic field, the distance between current source and target is critical as it directly affects the strength of the magnetic field. Fig.2 (a) shows the transverse view of the coil and it can be seen that one side of the coil blade will be located further away from the sample with the increment of the rotation angle of the blade.

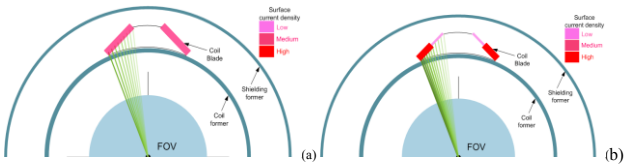

Figure 2(a) (Transverse view of a coil element) Illustration of the basic relationship between source and induced field. The surface current density on the coil blade is uniformly distributed; (b) Illustration of the basic relationship between source and induced field. The surface current distribution is concentrated on the one side of the coil blade.

In consideration of the above analysis, we optimized the structure design of the coil blade in an attempt to concentrate the surface current close to the sample, to try to improve the RF penetration depth (see Fig.2 (b)). A new stripline-like type of conductor for the coil element was developed [9]. In the new design, a single copper conductor is sandwiched between another two copper strips and dielectric materials, hence the name sandwich conductor. The comparison of the former design and the new 'sandwiched' design of the coil blade is shown in Fig. 3. This design for the conductor maintains the uniformly distributed capacitance and inductance in the blades, therefore containing the electric field and reducing coupling to the sample. On this sandwich designed rung, the resonant current first flows through the first part of the wide middle panel and then in parallel to the top and the bottom narrow conductors before reuniting again on the second part of the wide middle panel. As such, the resonant current flowing through the top and bottom layers was directed to one side of the coil blade, so that the aim of reducing the distance between current sources and the sample was achieved (as depicted in Fig.3 (b)). Additionally, the middle layer is still kept wide, in order to maintain the flux-steering technique of the angularly orientated coil element.

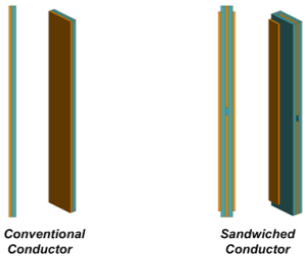

Figure 3 Comparison of the coil element structure between the conventional conductor structure and the novel sandwiched conductor structure

B. *Optimization of the coil structure configuration*

In addition, the configuration of the coil structure, including the rotation angle of the blade and the aperture size of the coil element, was further optimized with the consideration of an engineering trade-off between RF penetration and next-neighbour coil coupling. This means that each coil element of the array is configured to minimize leakage flux which cuts across the neighbouring coil element to reduce mutual coupling and to maximize flux coupling to the sample, producing maximal field contribution to the central imaging area.

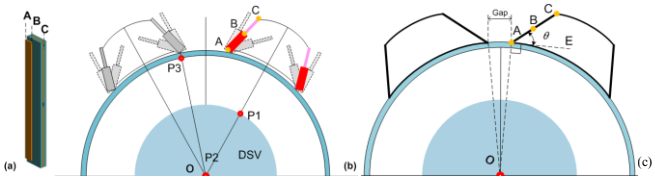

Figure 4 (a) A, B and C indicates three different positions on the transverse section of the coil blade. (b) (Transverse view of a coil element) Illustration of the coil structure optimization scheme. (c) Dimension of the coil structure on transverse view

To evaluate the magnetic field distribution induced by the coil element, three target field sampling points: P1, P2 and P3 were set on the boundary of the DSV, the centre of the DSV and the point on the neighbouring coil blade, respectively (see Fig. 4 (b)). In this circular 8-element array system, the field strength on the centre point P2 can be employed to indicate the coil penetration depth. The stronger the magnetic field on P2, the deeper the RF penetration of the coil. The sensitivity profile of the coil element is another important factor that should be considered when the transceive array coil operates in the receive mode. Hence, P2 and P1 are used to evaluate the field distribution so as to improve the reception capability of the coil. Then, to acquire information on the leakage flux of the coil, an observation point is set on position P3 to measure the magnetic field strength. Obviously, the weaker the magnetic field on P3, the lesser the leakage flux, and thus minimum mutual coupling occurs between the adjacent coils. Therefore, the optimization target is to realize maximum field

strength on observation points P1, P2, and minimum on P3. The design objective can be mathematically expressed as:

$$\min \{w_1/B_{p1} + w_2/B_{p2} + w_3 \bullet B_{p3}\}$$

Where, B_{p1}, B_{p2} and B_{p3} are the magnetic field on positions P1, P2 and P3 respectively; w_1, w_2, and w_3 are weighting coefficients of the minimization function. Nonlinear least-square optimization method is used to achieve the optimization aims [2, 10]. The coil structure changes with the variation of the angle θ and the Gap between two coils (see in Fig. 4(c)); hence, the field strength on those three observation positions will change accordingly. So, θ and Gap are the two variables in the optimization routine. For the field calculation, Biot-Savart law was employed to evaluate the magnetic field on these three preset points. Although Biot-Savart law will not adequately model the resonator at high frequency, this approach significantly simplifies the numerical calculation and also reveals the intrinsic physical property of this case in an easy way. It should be noted that in the employment of the Biot-Savart law, the surface current amplitude on section A-B (the top/bottom conductor) of the blade is much higher than on section B-C (the middle conductor), this conforms to the current distribution expected in the new structure (see in Fig. 4(a)(c)).

III. Results and Discussion

A. Validation of the numerical simulation

Upon obtaining the optimized results, the new coil element was modelled and simulated using the Electromagnetic software package FEKO. A comparison study on RF penetration using the sandwich conductor structure was undertaken. Shown in Fig.5 (a) is a coil element using the conventional conductor, Fig.5 (b) is a coil element using sandwich conductors as in our previous design, and Fig.5 (c) represents the coil element used for the new array with stripline-like sandwich conductor and larger loop aperture size. All the modelled coils are tuned to 400MHz (9.4T) and matched to 50Ω under loaded conditions. With a voltage source (amplitude: 1V; phase: 0degree) excitation, magnetic fields inside the phantom are calculated and compared. The effective RF penetration for these three coil elements is plotted and shown in Fig.5 (d). It can be observed that through using the new sandwich conductor structure the RF penetration can be increased (roughly 13%) and a further increment is noticed for the larger aperture sized loop (approximately 24% increase compared to the coil (a)).

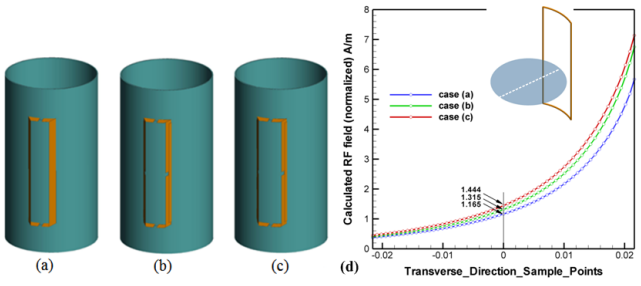

Figure 5 (a), (b) are the former and (c) new coil configuration; and (d) the comparison of normalized H-field along the transverse section centre of the phantom

For the RF coil design, the SNR is an important factor. The sample noise of these three coil designs, Fig.5 (a)-(c), is approximately the same. The SNR comparison of these three coils can be expressed by the evaluation of the signal reception capability. Using the principle of reciprocity, such a transceive coil used for transmission would have the same sensitivity profile for signal reception in receive mode. So we can understand the SNR of this coil design through the comparison of coil RF penetration to confirm that the new coil design (c) can achieve higher SNR than the others (coil (a)-(b)).

Upon using the angularly rotated coil blade technique which regulated the mutual coupling, a counter-wound inductor decoupling method [11] was additionally utilized, as shown. With an appropriate coupling area and adjustment of the distance between inductors, this technique can provide very good isolation power. The mutual coupling between the coils was around -24dB, which means each channel of the array coil was isolated very well and the mutual coupling has little effect on the magnetic field distribution.

B. Hardware fabrication and RF Field Penetration Comparison

To validate the improvement of RF field penetration of the newly designed coil element compared to that of the conventional loop coil element, comparison experiments were carried out. A prototype of a newly designed coil element and a comparable conventional loop coil element were constructed and are shown in Fig. 6 (a-b). To test the RF field strength, a network analyzer (Agilent E5062A) was used with a sensitive, wideband RF probe, shown in Fig. 6 (c). Both the newly designed coil element and a conventional element were tuned to resonate at 400MHz and matched to an impedance of 50 Ohm. The coil elements were connected in turn to port 1 of the network analyser and used as a transmit coil, and the RF probe was used as a receive coil by connecting to port 2 of the analyser. The amplitude of the RF signal acquired by the RF probe directly reflects the RF field penetration of the transmit coil.

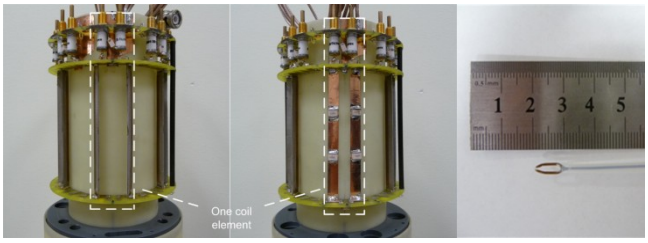

(a) (b) (c)

Figure 6 the constructed prototype of (a) a newly designed coil element and (b) a conventional loop coil (RF shields are removed for view), (c) the probe for RF signal acquisition

For comparison of the RF field penetration, three different experiments were performed. As shown in Fig.7 (a)-(c), the coil element was tested with or without loading. Two different cylindrical phantoms were used as the load and are shown in Fig.8. Both phantoms contain a saline solution (1.24g $NiSO_4 \bullet 6H_2O$ + 2.62g NaCl per 1 kg distilled water) and are 100mm long. Phantom 1 has a diameter of 53mm and is centered within the coil and phantom 2 has a diameter of

60mm and is offset towards the RF coil loop element as shown in Fig.7. In cases (a) and (b), the testing point *P* is located at the centre, and in case (c), it is located on the surface of the phantom.

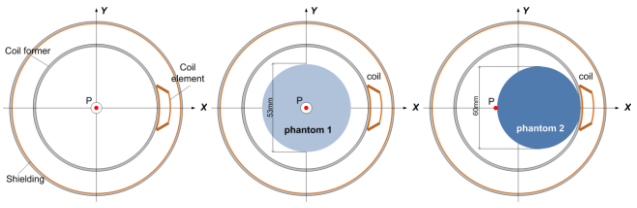

(a) (b) (c)

Figure 7 Illustration of three different RF field penetration experiments, (a) without loading, (b) loading with phantom 1 and (c) loading with phantom 2. P is the testing point where the RF probe is located.

(a) (b)

Figure 8 Cylindrical phantoms, **(a)** phantom 1 and **(b)** phantom 2

Fig.9 shows the comparison of RF field penetration between the newly designed coil element and the conventional loop coil by simulation and experiment. The experimental results show that the RF field strength of the new design is improved by 24.45% compared with the conventional loop coil in case (a), and 25.89% in case (b), and 14.82% in case (c). It can also be seen that the corresponding experiment results are consistent with the simulations.

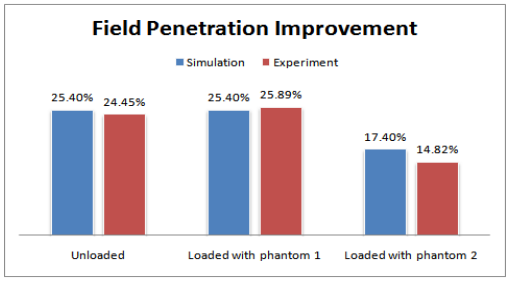

Figure 9 the calculated and tested field strength improvement of the newly designed coil compared to that of a conventional coil element

C. *Imaging experiment*

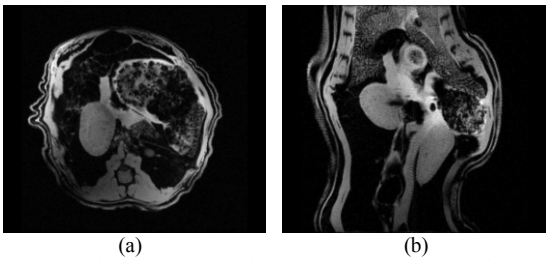

(a) (b)

Figure10 axial (a) and coronal (b) section rat images through kidneys

The prototype transceive array system was tested in a Bruker 9.4T Biospec MRI system and MR images were acquired. Fig. 10 (a) and (b) are axial and coronal FLASH images of a rat abdomen obtained with fat suppression. The kidney can clearly be seen directly above the intense fat signal region.

IV. Conclusion

In this work, a dedicated 8-channel transceive volume array for small animal MRI applications at 9.4T was developed. The array was designed within the limited space available by using a dedicated coil structure which contains angularly oriented conductive coil elements with stripline-like, 'sandwich' conductors. The design allows the use of large coil aperture, minimize coil-coil coupling and capacitive coil-sample coupling. Therefore the design offers good coil performance including exceptional field penetration, minimal signal coupling between elements and a high coil efficiency. Both simulation and experimental results clearly demonstrate the advantages of the proposed novel array configuration. Future work will investigate the potential of this design for larger and denser coil array configurations for both animal and human imaging.

References

[1] Li, B.K., B. Xu, F. Liu, and S. Crozier, *Multiple-acquisition parallel imaging combined with a transceive array for the amelioration of high-field RF distortion: A modeling study.* Concepts in Magnetic Resonance Part B: Magnetic Resonance Engineering, 2006. 29B(2): p. 95-105.

[2] Liu, F., B.L. Beck, J.R. Fitzsimmons, S.J. Blackband, and S. Crozier, *A theoretical comparison of two optimization methods for radiofrequency drive schemes in high frequency MRI resonators.* Physics in Medicine and Biology, 2005. 50(22): p. 5281-5291.

[3] Li, B.K., F. Liu, and S. Crozier, *Focused, eight-element transceive phased array coil for parallel magnetic resonance imaging of the chest- : Theoretical considerations*. Vol. 53. 2005, Baltimore, MD, ETATS-UNIS: Williams & Wilkins. 7.

[4] Roemer, P.B., W.A. Edelstein, C.E. Hayes, S.P. Souza, and O.M. Mueller, *The Nmr Phased-Array.* Magnetic Resonance in Medicine, 1990. 16(2): p. 192-225.

[5] Zhang, X. and A. Webb, *Design of a capacitively decoupled transmit/receive NMR phased array for high field microscopy at 14.1 T.* Journal of Magnetic Resonance, 2004. 170(1): p. 149-155.

[6] Wu, B., X.L. Zhang, P. Qu, and G.X. Shen, *Design of an inductively decoupled microstrip array at 9.4 T.* Journal of Magnetic Resonance, 2006. 182(1): p. 126-132.

[7] Lee, R.F., R.O. Giaquinto, and C.J. Hardy, *Coupling and decoupling theory and its application to the MRI phased array.* Magnetic Resonance in Medicine, 2002. 48(1): p. 203-213.

[8] Weber, E., B.K. Li, F. Liu, and S. Crozier, *A Ultra High Field Multi-Element Transceive Volume Array for Small Animal MRI.* 2008 30th Annual International Conference of the Ieee Engineering in Medicine and Biology Society, Vols 1-8, 2008: p. 2039-2042 5942.

[9] Li, Y., E. Weber, B. Li, F. Liu, J. Schneider, S. Ohrel, S. Junge, P. Ullmann, M. Wick, and S. Crozier, *A Stripline-like Coil Element Structure for High Field Phased Array Coils and its Application for a 8-channel 9.4T Small Animal Transceive Array.* Proceedings of the 16th Annual Meeting of ISMRM, 2010: p. 151.

[10] Branch, M.A., T.F. Coleman, and Y. Li, *A Subspace, Interior, and Conjugate Gradient Method for Large-Scale Bound-Constrained Minimization Problems.* SIAM J. Sci. Comput., 1999. 21(1): p. 1-23.

[11] Crozier, S., B.K. Li, and E. Weber, *"MRI Coil Decoupling"*, I.B. World Intellectual Property Organization, Editor. 2008.